

MODELLING OF THREE PORT DC TO DC CONVERTER FOR STAND ALONE PHOTO VOLTAIC POWER SYSTEM

***G ASHWINI, **CH RAJU**

*PG Scholar, Department Of EEE, Vaagdevi College of Engineering(UGC-Autonomous, Accredited By NBA)

**Assistant Professor, Department of EEE, Vaagdevi College Of Engineering(UGC-Autonomous, Accredited By NBA)

ABSTRACT:

The System efficiency and cost effectiveness are of critical importance for photovoltaic (PV) systems. This project addresses the two issues by developing a novel three- port DC-DC converter for standalone PV systems, based on an improved Fly back-Forward topology. It provides a compact single unit solution with a combined feature of optimized maximum power point tracking (MPPT), high step-up ratio, galvanic isolation and multiple operating modes for domestic and aerospace applications. A theoretical analysis is conducted to analyze the operating modes. This project is focused on a comprehensive modulation strategy utilizing both PWM and phase-shifted control that satisfies the requirement of PV power systems to achieve MPPT and output voltage regulation. A 500 W converter was designed and simulation results are verified by using MATLAB-SIMULINK in terms of system integration and high conversion efficiency.

INTRODUCTION:

It is expected that distributed renewable energy sources will be more and more used in the future electric grid. Power converters will play an important role in interfacing the renewable energy sources and the electric grid and load [1]. The power management and grid integration of multiple energy sources are commonly realized by using multiple individual converters. Compared to that solution, using an integrated multiport converter is preferable since it has less components and a higher power density [2]-[5]. Besides, it requires no communication capabilities that would be necessary for multiple individual converters. Depending on their voltage levels, the renewable energy sources are usually connected to an electric grid or a load through a one-stage or a two-stage power converter system. For the applications where the voltage of the renewable energy source is low, an isolated multiport DC-DC converter is preferred to be used in a two-stage

power converter system, as shown in Fig. 1. The isolated multiport DC-DC converter has multiple input ports for connecting different sources and multiple functions. It not only regulates the low-level DC voltages of the sources to a constant high level required by the inverter, but also can provide other important control functions, such as maximum power point tracking (MPPT), for the renewable energy sources.

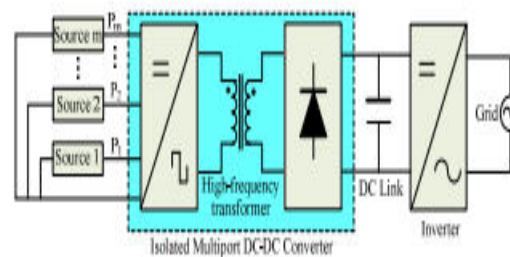


Fig. 1. Configuration of a two-stage, grid-connected, multisource energy system.

Due to the intermittence of the renewable energy sources, an energy storage device, such as a battery, is commonly used with the renewable energy sources. In such a hybrid energy system, a multiport converter with at least one bidirectional port, namely, a multiport bidirectional converter is required to interface the storage device. A variety of multiport bidirectional DC-DC converters has been proposed for twostage grid integration of renewable energy sources [6]-[10]. These topologies either use too many active switches or have a negative effect on the battery lifetime due to the highfrequency charge/discharge for the battery. For example, in [10], the battery was both charged and discharged within a switching period. Such a high-frequency charge/discharge has a negative effect on the battery lifetime. Recently, a new multiport bidirectional DC-DC converter with the least number of switches has been proposed [11]. In that converter, the battery was charged and discharged at a low frequency and the main switch could be turned off under the zero-current switching (ZCS) condition using a resonant circuit. However, the two switches in the bidirectional port are still hard switched. In this paper, an isolated three-port DC-DC converter (TPC) is proposed. Compared with the TPC in [11], the proposed TPC has the same number of the switch and all the switches can be turned on under the zero-voltage switching (ZVS) condition. Since a multiport converter is a multi-input multi-output (MIMO) system, a decoupling technique is desired to control different state variables of the system independently [6]. This paper presents a small signal model for the proposed TPC. Based on the model, two controllers are designed to regulate the power flows of the two sources and the output voltage of the TPC. Experimental results are provided to validate the proposed controllers when the TPC works in different conditions.

PRINCIPLE OF OPERATION

This section introduces the topology of proposed non isolated three-port dc-dc converter, as illustrated in Fig. 2. The converter is composed of two main switches S_1 and S_2 for the battery and PV port. Synchronous switch S_3 is driven complementarily to S_1 such that bidirectional power flow for the battery port can be achieved. Two coupled inductors with winding ratios n_1 and n_2 are used as voltage gain extension cells. Two sets of active clamp circuits formed by S_4, Lk_1, Cc_1 and S_5, Lk_2, Cc_2 are used to recycle the leakage energy. Lk_1 and Lk_2 are both composed of a small leakage inductor from the coupled inductor and an external leakage inductor. Two independent control variables, duty cycles d_1 and d_2 , allow the control over two ports of the converter, while the third port is for the power balance. The fixed-frequency driving signals of the auxiliary switches S_3 and S_4 are complementary to primary switch S_1 . Again, S_3 provides a bidirectional path for the battery port. Similarly, S_5 is driven in a complementary manner to S_2 . A 180° phase shift is applied between the driving signals of S_1 and S_2 .

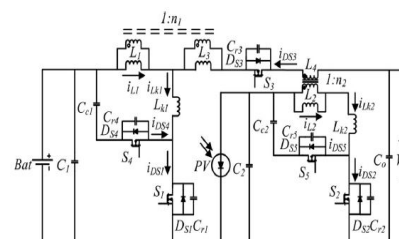


Fig 2. Topology of the proposed converter

There are four operation periods based on the available solar power. First, the sun is in the eclipse stage and the solar irradiation is either unavailable or very low. This operation period is defined as period 1, and the battery will serve as the main power source. As the sun

starts to shine and the initial solar irradiation is enough for supplying part of the load demand, the Operation period is changed to period 2. The load is supplied by both solar and battery power in this period. For period 3, the increasing isolation makes the solar power larger than the load demand. The battery will preserve extra solar power for backup use. During period 4, the charging voltage of the battery reaches the preset level and should be limited to prevent overcharging. According to the solar irradiation and the load demand, the proposed three-port converter can be operated under two modes. In the battery balance mode (mode 1), maximum power point tracking (MPPT) is always operated for the PV port to draw maximum power from the solar panels. The battery port will maintain the power balance by storing the unconsumed solar power during light-load condition or providing the power deficit during heavy-load condition. The power sharing of the inputs can be represented as

$$P_{load} = P_{pv\ SVC} + P_{bat\ SVC}$$

Where p_{load} is the load demand power, $P_{PV\ SVC}$ is the PV power under solar voltage control (SVC), and $P_{bat\ SVC}$ is the battery power under SVC.

In mode 1, maximum power is drawn from the PV source. The battery may provide or absorb power depending on the load demand. Therefore, $P_{bat\ SVC}$ could be either positive or negative. When the battery charging voltage is higher than the maximum setting, the converter will be switched into battery management mode (mode 2). In mode 2, MPPT will be disabled; therefore, only part of the solar power is drawn. However, the battery voltage could be controlled to protect the battery from overcharging.

The power sharing of the inputs can be represented as

$$P_{load} = P_{pv\ BVC} + P_{bat\ BVC}$$

Where PV_{BVC} is the PV power under battery voltage control (BVC) and $P_{bat\ BVC}$ is the

battery charging power under SVC. If the load is increased and the battery voltage is reduced, the Converter will be switched to mode 1. The output voltage is always kept at 380 V in both modes.

OPERATION OF THE TOPOLOGICAL MODES

Before performing the analysis, some assumptions should be made:

- 1) The switches are assumed to be ideal
- 2) The magnetizing inductors are large enough so that the current flowing through the inductors is constant;
- 3) The capacitors are large enough so that the voltages across the capacitors are constant. The topological modes over a switching cycle are shown in Fig. 4 and key waveforms of the proposed converter are given in Fig. 5. Detailed explanation of each interval is given as follows:

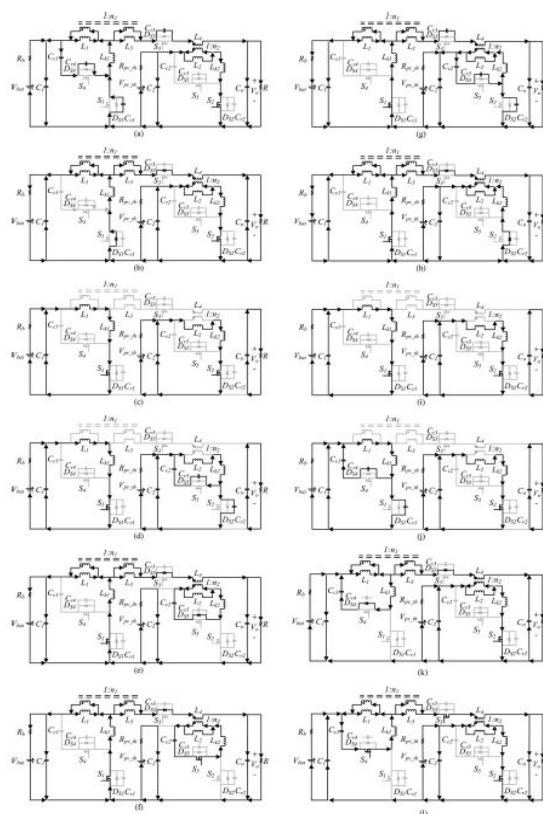


Fig4.2. Topological modes of the proposed converter.

(a) Interval 1. (b) Interval 2. (c) Interval 3. (d) Interval 4. (e) Interval 5. (f) Interval 6. (g) Interval 7. (h) Interval 8. (i) Interval 9. (j) Interval 10. (k) Interval 11. (l) Interval 12.

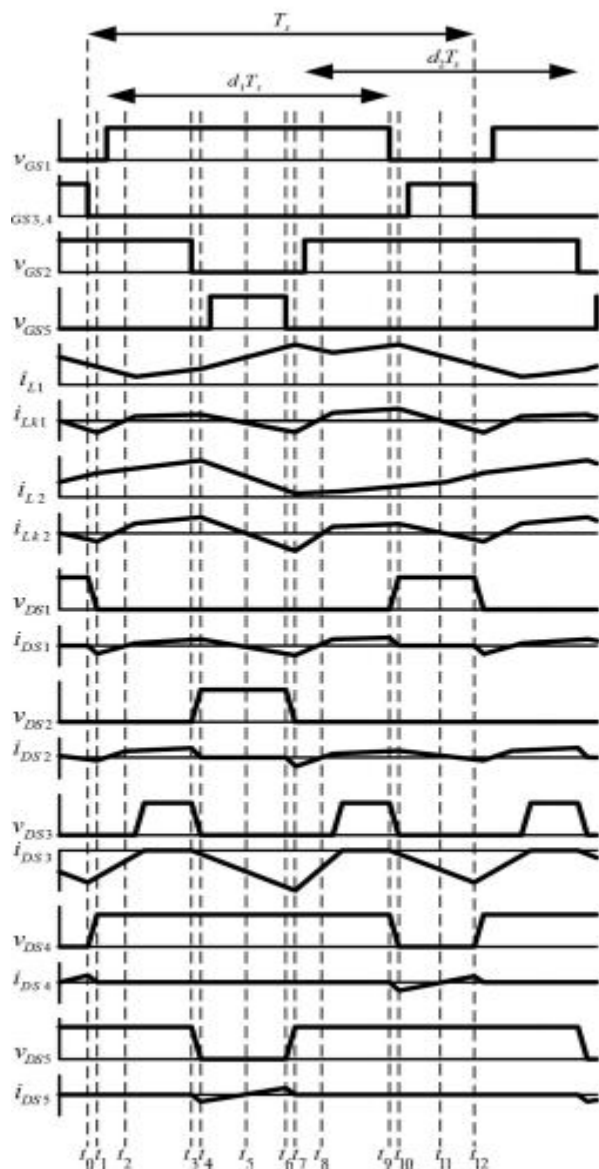


Fig 4.3.Key waveforms of the designed converter.

Interval 1 [see Fig. 4(a), $t_0 \leq t < t_1$]: At t_0 , S1 and auxiliary switches S4 and S5 are turned OFF, while primary switch S2 is turned ON. Although S1 is in the off state, resonant inductor Lk1 resonates with Cr1 and Cr4. In this period,

Cr1 is discharged to zero and Cr4 is charged to $V_{bat} + V_{Cc1}$. For the PV port, S2 is turned ON and the current from the PV panels flows through VPV Th– L2 – Lk2 – S2 loop. In order to achieve the ZVS feature for S1, the energy stored in resonant inductor Lk1 should satisfy the following inequality

Interval 2 [see Fig. 4(b), $t_1 \leq t < t_2$]: This mode starts when v_{ds1} is down to zero. The body diode of S1 is forward biased so that the ZVS condition for S1 is established. The resonant current i_{Lk1} is increased toward zero. L2 is still linearly charged in this period.

Interval 3 [see Fig. 4(c), $t_2 \leq t < t_3$]: S1 begins to conduct current at t_2 and the battery port current follows the path $V_{bat} - L1 - Lk1 - S1$. S2 is also turned ON in this interval. Therefore, Both L1 and L2 are linearly charged and energy of both input ports is stored in these magnetizing inductors. Auxiliary switches S3, S4, and S5 are all turned OFF.

Interval 4 [see Fig. 4(d), $t_3 \leq t < t_4$]: In this interval, S2 starts to be turned OFF and the auxiliary switch S5 remains in the OFF state. However, a resonant circuit formed by Lk2, Cr2, and Cr5 releases the energy stored in Lk2. Resonant capacitor Cr2 is quickly charged to $VPV Th + V_{Cc2}$, while Cr5 is discharged to zero. In order to achieve the ZVS feature for S5, the energy stored in resonant inductor Lk2 should satisfy the following inequality:

$$L_{k2} \geq \frac{(C_{r2} || C_{r5}) [v_{DS5}(t_3)]^2}{[i_{Lk2}(t_3)]^2} \quad (30)$$

Interval 5 [see Fig. 4(e), $t_4 \leq t < t_5$]: At t_4 , v_{DS5} reaches zero and the body diode across the auxiliary switch S5 is turned ON. Therefore, a ZVS condition for S5 is established. Given that the Cr5 is much smaller than Cc2, almost all the magnetizing currents are recycled to charge the clamp capacitor Cc2. Furthermore, V_{Cc2} is considered as a constant value since the capacitance of Cc2 is large enough. This interval ends when inductor current i_{Lk2} drops to zero.

Interval 6 [see Fig. 4(f), $t_5 \leq t < t_6$]: At t_5 , the current of L_{k2} is reversed in direction and energy stored in t_5 is released through the C_{c2} - S_5 - L_{k2} - L_3 loop. This interval ends when S_5 is turned OFF.

Interval 7 [see Fig. 4(g), $t_6 \leq t < t_7$]: Switches S_2 and S_5 are both in the OFF state at t_6 . A resonant circuit is formed by L_{k2} , C_{r2} , and C_{r5} . During this interval, C_{r2} is discharged to zero and C_{r5} is charged to $V_{PV} + V_{C_{c2}}$. To ensure the ZVS switching of S_2 , the energy stored in L_{k2} should be greater than the energy stored in parasitic capacitors C_{r2} and C_{r5}

$$L_{k2} \geq \frac{(C_{r2} || C_{r5}) [v_{DS2}(t_6)]^2}{[i_{L_{k2}}(t_6)]^2}$$

Interval 8 [see Fig. 4(h), $t_7 \leq t < t_8$]: This interval starts when the voltage across C_{r2} is zero and the body diode DS_2 is turned ON. Leakage inductor current $i_{L_{k2}}$ is linearly increased and the secondary-side current of the coupled inductor is increased as well. The main switch S_2 should be turned ON before $i_{L_{k2}}$ becomes positive to ensure ZVS operation.

Interval 9 [see Fig. 4(I), $t_8 \leq t < t_9$]: The circuit operation of interval 9 is identical to interval 3 since S_1 and S_2 are turned ON in both intervals.

Interval 10 [Fig. 4(j), $t_9 \leq t < t_{10}$]: At t_9 , S_1 is turned OFF, while S_3 and S_4 remain in OFF state. During this interval, L_{k1} will resonate with C_{r1} and C_{r4} to release the energy trapped in it. Resonant capacitor C_{r1} is charged to $V_{bat} + V_{C_{c1}}$, while C_{r4} is discharged to zero. To achieve the ZVS feature for S_4 , the energy stored in resonant inductor L_{k2} should satisfy the following inequality:

$$L_{k1} \geq \frac{(C_{r1} || C_{r4}) [v_{DS4}(t_9)]^2}{[i_{L_{k1}}(t_9)]^2}$$

Interval 11 [see Fig. 4(k), $t_{10} \leq t < t_{11}$]: This interval begins when v_{DS4} drops to zero and the body diode across S_4 is turned ON. The ZVS condition for S_4 is then established. Almost all the magnetizing current is recycled

to charge C_{c1} since C_{r4} is much smaller than C_{c1} . Moreover, $V_{C_{c1}}$ is considered as a constant value since the capacitance of C_{c1} is large enough. This interval ends when inductor current $i_{L_{k1}}$ reaches zero.

Interval 12 [see Fig. 4(l), $t_{11} \leq t < t_{12}$]: The current flow through L_{k1} is reversed in direction at t_{11} , and the energy stored in C_{c1} is released through the C_{c1} - S_4 - L_{k1} - L_1 loop. This interval ends when S_4 is turned OFF and the operation of the proposed converter over a switching cycle is complete.

SIMULATION RESULTS

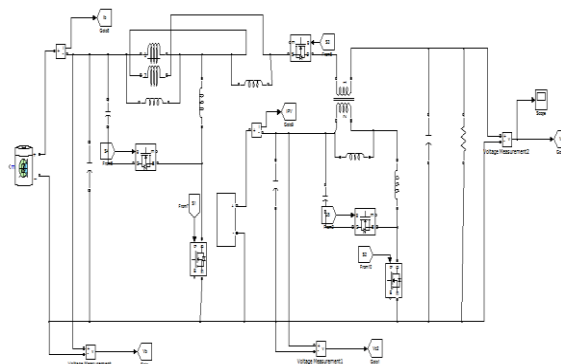


Fig 6.1 MATLAB/SIMULINK circuit diagram of designed three port DC-DC converter

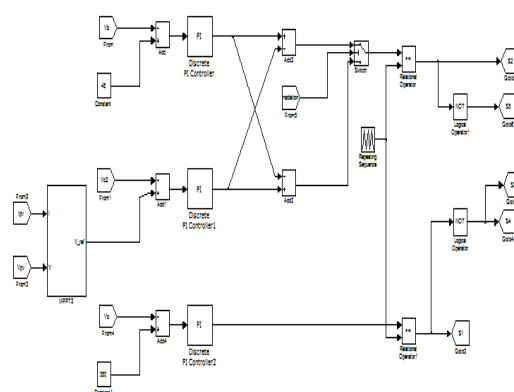


Fig 6.2 Controller subsystem

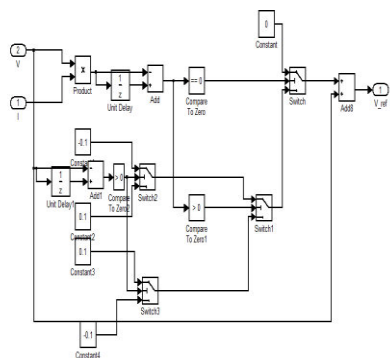


Fig 6.3 Maximum power point tracking circuit

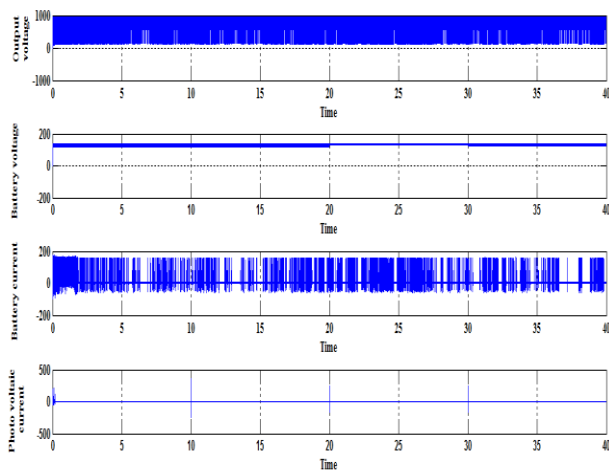


Fig 6.4 Simulation Results of the designed control scheme

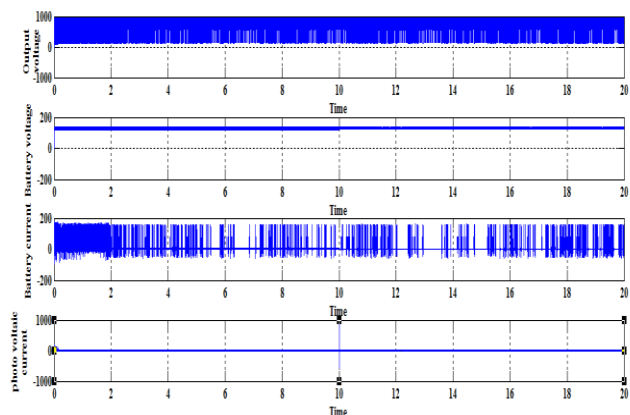


Fig 6.5 Experimental results of the designed converter

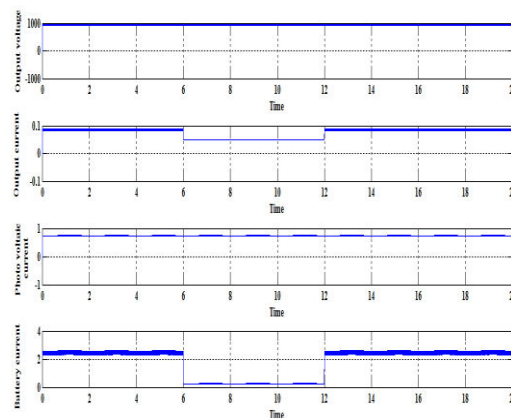


Fig 6.6 Results for the change of load

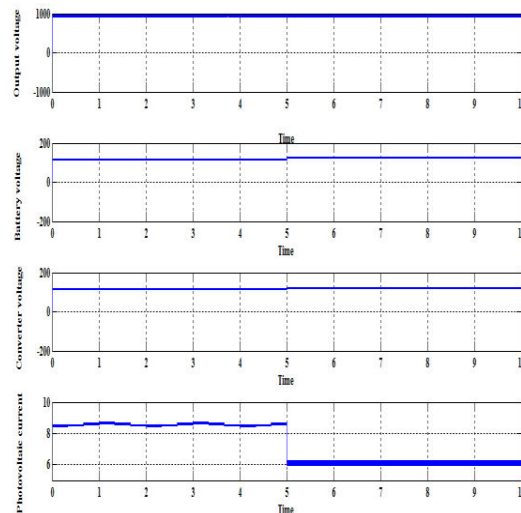


Fig 6.7 Results from mode 1 to 2

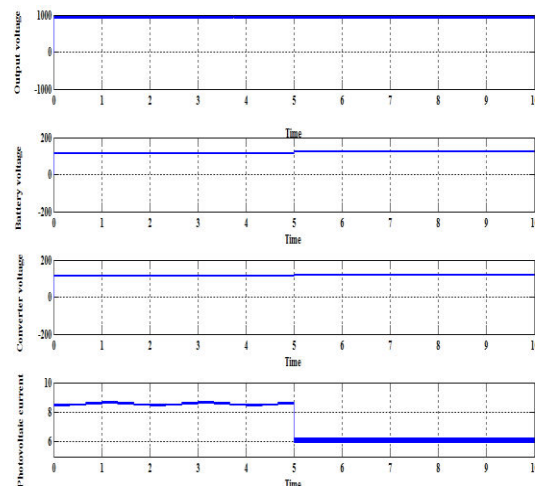


Fig 6.8 Results from mode 2 to 1

CONCLUSION

A high step-up three-port DC–DC converter for stand-alone power systems is proposed to integrate solar and battery power. In the proposed topology, two coupled inductors are employed as voltage gain extension cells for high voltage output applications. Two sets of buck–boost type active-clamp circuits are used to recycle the energy stored in the leakage inductors and improve the efficiency. The proposed switching strategy only needs to control two duty ratios in different operation modes. The experimental results validate the functionality of the proposed converter under different solar irradiation level and load demand. The charging/discharging transitions of the battery could be achieved without changing the operation mode; therefore, the MPPT operation will not be interrupted. In light-load condition, once the charging voltage is higher than the present level, the operation mode will be changed rapidly to protect the battery from overcharging. The highest converter efficiency is measured as 90.1% at 110W. The control method of the battery port could be modified for the grid-connected applications. Discussion from control viewpoints including moving the effect of RHP-zeros to particular output, limitations on sensitivity of the system, tradeoffs in the feedback controller design, and implementation of an improved decoupling method should be presented in our future work.

REFERENCES

- [1] S. H. Chong and A. Kwasinski, "Multiple-input DC-DC converter topologies comparison," in Proc. 34th Annu. Conf. IEEE Ind. Electron., 2008, pp. 2359–2364.
- [2] A. Huang, "FREEDM system—a vision for the future grid," in Proc. IEEE Power Energy Soc. Gen. Meet., 2010, pp. 1–4.
- [3] W. Li and X. He, "Review of no isolated high-step-up DC/DC converters in photovoltaic grid-connected applications," IEEE Trans. Ind. Electron., vol. 58, no. 4, pp. 1239–1250, Apr. 2011.
- [4] T.-F. Wu, Y.-S. Lai, J.-C. Hung and Y.-M. Chen, "Boost converter with coupled inductors and buck–boost type of active clamp," IEEE Trans. Ind. Electron., vol. 55, no. 1, pp. 154–162, Jan. 2008.
- [5] W. G. Imes and F. D. Rodriguez, "A two-input tri-state converter for spacecraft power conditioning," in Proc. AIAA Int. Energy Converts. Eng. Conf., 1994, pp. 163–168.
- [6] F. D. Rodriguez and W. G. Imes, "Analysis and modeling of a two input DC/DC converter with two controlled variables and four switched networks," in Proc. AIAA Int. Energy Conf., 1994, pp. 163–168.
- [7] B. G. Dobbs and P. L. Chapman, "A multiple-input DC–DC converter topology," IEEE Power Electron. Lett. vol. 1, no. 1, pp. 6–9, Mar. 2003.
- [8] R. J. Wai, Ch. Y. Lin, J. J. Liaw, and Y. R. Chang, "Newly designed ZVS multi-input converter," IEEE Trans. Ind. Electron., vol. 58, no. 2, pp. 555–566, Feb. 2011.
- [9] L. Solero, A. Lidozzi, and J. A. Pomilio, "Design of multiple-input power converter for hybrid vehicles," in Proc. IEEE Appl. Power Electron. Conf., 2004, pp. 1145–1151.
- [10] F. Nejabatkhah, S. Danyali, S. H. Hussein, M. Sabah, and S. M. Niapour, "Modeling and control of a new three-input DC-DC boost converter for hybrid PV/FC/battery power system," IEEE Trans. Power Electron., vol. 23, no. 2, pp. 782–792, Mar. 2008.
- [11] J. Jung and A. Kwasinski, "A multiple-input SEPIC with a bi-directional input for modular distributed generation and energy storage integration," in Proc. IEEE Appl. Power Electron. Conf., 2011, pp. 28–34.
- [12] G.-J. Su and F. Z. Peng, "A low cost, triple-voltage bus DC–DC converter for automotive applications," in Proc. IEEE Appl. Power Electron. Conf., 2005, pp. 1015–1021.